Assessment of ultrasound source localization accuracy on damaged and healed concrete

Eleni Tsangouri[1, 2*], Grigorios Karaiskos[1], Arnaud Deraemaeker[3],

Danny Van Hemelrijck[1], Dimitrios Aggelis[1]

[1] Vrije Universiteit Brussel, Mechanics of Materials and Constructions (MeMC), Brussels, Belgium

[2] SIM Flanders, Zwiinaarde, Ghent, Belgium

[3] Université Libre de Bruxelles (ULB), BATir Laboratory, Brussels, Belgium

* Corresponding author: etsangou@vub.ac.be

Abstract: The accuracy of ultrasound source localization is measured on damaged and autonomously healed concrete. A piezoelectric transducer is fixed into concrete and emits high-amplitude and short-duration pulses transformed into complex stress waves as they travel through concrete (pulse transmission). Eight Acoustic Emission (AE) sensors, attached on concrete surface, locate the pulse source spatially and chronically. It is shown that the transmitter localization progressively loses its accuracy with 3D spatial error up to 15% in the presence of crack 300 μm wide. The source localization error diminishes to 3.4% as the crack autonomously heals. The study aims at developing a monitoring system that accurately senses damage and can be applied on the next generation of smart engineering concrete in order to autonomously and repeatedly repair its cracks through piping network with supply of healing agent.

Keywords: Ultrasound wave, concrete, acoustic emission, embedded piezoelectric transducer, damage, autonomous healing, wave source localization

1. INTRODUCTION

1.1 The monitoring techniques at the service of autonomous healing

Traditionally, once a crack is accurately detected in concrete [1], repairing additives are manually injected into the crack void [2]. Sealing and partial superficial restoration is obtained because the additives cannot easily penetrate throughout the entire crack's depth. Autonomously healed concrete, developed the last decade, aim at replacing the manual repair agent injection by embedding encapsulated repair agent into concrete during casting. The healing process is activated only in the nucleation and extension of a crack that ruptures the brittle capsule and triggers the release of the agent into the crack void [3]. The latter repair method is more efficient than the previous manual processes since the crack is automatically filled internally and the restoration is accomplished at the early damage stage.

Different monitoring techniques are involved in order to evaluate the repair efficiency of these smart healing processes [4]. In previous studies, the conditions under which the healing is triggered are assessed by Acoustic Emission (AE) that detects the source location of the acoustic wave emitted as the capsule ruptures [4]. In addition, the ultrasound pulse velocity technique utilizes the emission of a pulse from a piezoelectric transducer (i.e. transmitter), that travels throughout the material and is received by a similar piezoelectric transducer (i.e. receiver). The received signal is used to quantify the structural integrity of concrete beams that are autonomously healed [5]. Additionally, the use of digital image correlation (DIC) provides an accurate localization of healed areas on concrete

[6]. The assessment of healing mechanisms on concrete becomes complicated in the presence of several cracks. In this case, cracks form, widen and close (due to healing) simultaneously. An integrated monitoring system that combines the DIC and AE techniques has been used in previous studies to monitor the progressive damage evolution of several cracks on concrete [7].

Nowadays and based on the well-established combination of the autonomously repaired concrete with integrated monitoring experimental methods, the next generation of self-repairing concrete is introduced namely self-healing vascular network concrete. The intelligent material design considers a sensing system (by means of optical or acoustic sensors) that detects damage and a piping network embedded into concrete that continuously supplies repair agent at any place across the concrete structure achieving repeatable autonomous crack restoration [8]. The distribution of the healing agent at different locations and at specific moments in time when appropriate, requires the presence of an inspecting mechanism that detects and triggers the healing activation and thus guarantees repeatable repair of concrete. The key features of this innovative technology applied on concrete is the timely warning when cracks appear or propagate, their accurate localization and the evaluation of the damage level obtained by use of advanced monitoring systems [8]. The accuracy of the sensing information, contributes to the cost-efficiency and long term repair of the crack [9].

1.2 Focus on the acoustic emission technique: the challenge due to concrete complex fracture

In literature, there is extensive research done evaluating the damage on concrete using acoustic wave propagation technique either in active (ultrasonics) or passive (AE) form [10-12]. Several techniques, based on the longitudinal or

Rayleigh wave velocity [13], the acoustic emission [14], the elastic wave tomography [15], are well-established providing accurate damage localization.

Wave source localization performs well in sound specimens even though concrete cannot be considered as a homogeneous material. The material components widely vary in size: the aggregates may have a diameter greater than 10 mm and the sand or other additives may have a diameter lower than 1 mm. The metal bar/fiber reinforcement and the potential encapsulated healing agent/embedded agent network contribute to the material's heterogeneity. Still in literature the location of damage in sound specimens or structures has been detected with suitable engineering accuracy [16, 17]. However, the damage development complicates the wave propagation on concrete and concrete composites [18, 19], reducing the wave transmission and speed characteristics. Due to quasi-brittle concrete nature, the fracture process initiates with micro-crack defects that accumulate forming macro-cracks that arrest or propagate and interact with other defects/cracks in the vicinity [20]. Taking into account that the knowledge of the elastic wave speed is crucial for the source localization, it is certain that the accuracy of source localization is compromised.

This study aims to investigate whether the source localization accuracy is suitable as a guide for repair in a self-healing network even at severely cracked conditions. The case of a plain pre-cracked concrete beam under mode-I fracture is considered. The emission source is an embedded aggregate-size piezoelectric transducer that is fed by a short-duration and high-amplitude voltage pulse. The localization accuracy in the presence of a crack that nucleates, propagates and is sealed after autonomous healing activation is evaluated.

2. MATERIALS AND TESTING METHODS

Lab-scale plain concrete beams of size 840 mm * 100 mm * 100 mm were fabricated. The concrete mixture composition is given in Table 1. A rectangular-shaped notch (pre-crack) with 10 mm height and 3 mm width at the middle section of the concrete beam is introduced in order to control crack initiation (single-edge notched beam). The design of concrete samples is based on Rilem TC-50 FMC protocol and is presented in Figure 1 [21].

Table 1. The concrete mixture.

Concrete composition	Content
Sand 0/4	670 kg/m^3
Gravel 2/8	490 kg/m^3
Gravel 8/16	790 kg/m^3
Cement CEM I 52.5 N	300 kg/m^3
Water	150 lt/m^3

A Crack Mouth Opening Device is attached at the two sides of the pre-crack groove and measures the crack opening at the bottom line of the beam. A the three-point bending test was performed till the opening of the crack is up to 0.3 mm wide (serviceability limit state design) and then the specimen was unloaded. The test is deflection controlled at the centerline of the beam with a loading rate of 0.05 mm/min. One concrete beam was cast carrying no healing agent (reference series: REF) and three more beams were cast with the encapsulated agent (healing series: PU1, PU2, PU3). The agent used in this study is a two-component adhesive polyurethane-based resin that polymerizes in the presence of moisture. The two components (adhesive and polymerization accelerator) were encapsulated into borosilicate glass spherical carriers 50 mm long, with 3.3 mm outer diameter and 3 mm inner diameter. The glass capsules break as a crack transverses and the adhesive components are released into the crack void. The polymerization process lasts few hours and the final product is a rigid and strong interlayer of polyurethane that fills the crack. A schematic representation of glass capsules is given in Figure 1 and the healing composition is summarized in Table 2. After the loading test, the concrete beam rests at the natural position (the crack opening stops at 0.25 mm approximately) and the healing agent polymerization occurs (agent curing time up to 24 hours). The loading test is repeated under the same testing configurations. At this reloading cycle the mechanical performance of the healed specimen is evaluated.

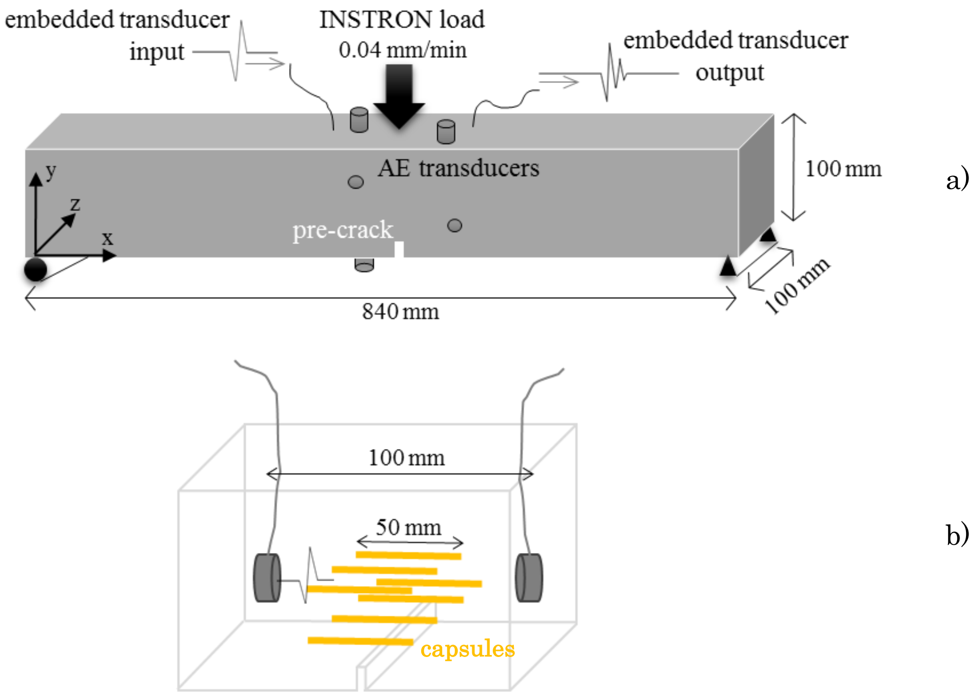

Figure 1. The concrete beam set-up: **a)** The side view of the specimen and the configuration of AE sensors. (The wires at the top side are connected to the embedded transducers; **b)** the interior of the central area: the long tubular borosilicate glass capsules (in yellow) are placed above the notch and the embedded piezoelectric transducers (colored in grey) are fixed at either side of the notch.

Table 2. The healing agent set-up.

Healing agent	2-component (precursor and accelerator) polyurethane agent
Carrier	Tubular borosilicate glass capsules 50 mm length / 3.3 mm outer diameter / 3 mm inner diameter
Carrier position	2series: 4 capsules pairs – 25 mm high 3 capsules pairs – 40 mm high from bottom
Crack volume	1000 mm^3
Released agent volume	3500 - 4000 mm^3

3. MONITORING TECHNIQUES SET-UP

3.1 Ultrasonic pulse velocity

An alternative to traditional ultrasound testing on concrete appears when the sensors attached on the material surface are replaced by low-cost and aggregate-size transducers embedded into the concrete while casting. This technique is based on the Smart Aggregates (SMAG) concept initially developed at the University of Houston [22, 23]. The advantage of embedded transducers is that good coupling conditions are guaranteed and do not vary depending on the couplant and pressure on the sensor as may be the case for surface mounting of sensors.. The embedded transducers consist of a flat piezoelectric lead-zirconate-titanate (PZT) patch of size 12 mm * 12 mm * 0.2 mm, which is wrapped by waterproof coating.

The electrical signals are transmitted to and from the transducer through electrical wires, which are conductively glued on both faces of the PZT patch. In our study, a pair of transducers is embedded into the concrete specimen. The transducers are fixed on each side of the center of the beam at a distance of 100 mm (Figure 2). One of the transducers emits a high voltage and short duration pulse (rectangular-shaped with 800 V magnitude and pulse width of 2.5 μs) that is transmitted through concrete (transmitter). The high-amplitude, spike-shaped signal excites the transducer to vibrate and this vibration excites the material through contact and generates stress waves. The stress waves propagate through concrete and are captured by all AE sensors and the second embedded transducer (receiver).

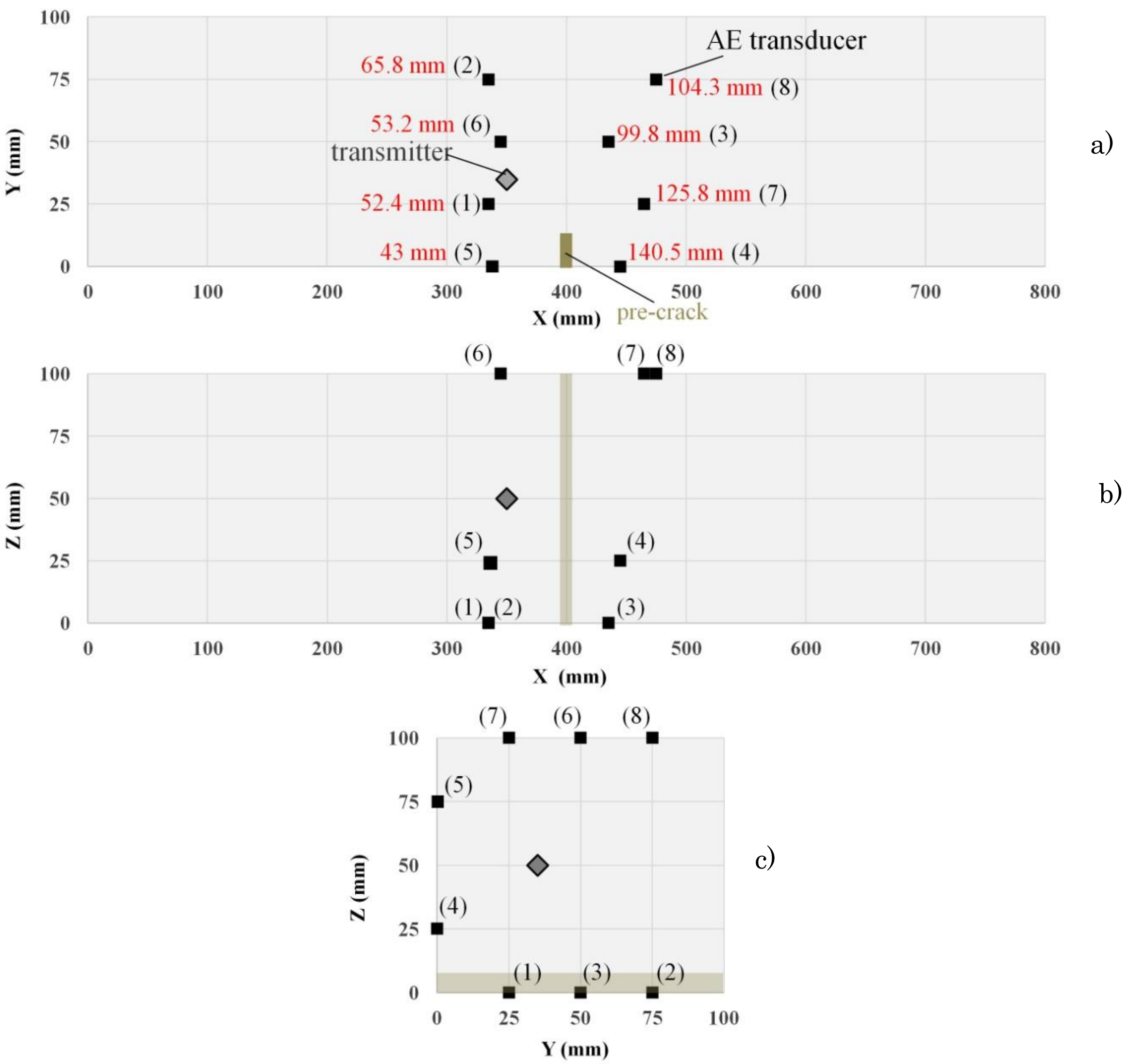

Figure 2. The AE sensors and the embedded transmitter set-up: **a)** The x-y; **b)** the x-z; **c)** the y-z plane projection. The transmitter is colored grey and the group of eight AE sensors are marked with black.

The position of the transmitter (shown in Figure 2 with grey rhombs) was initially chosen for the ultrasonic monitoring of autonomous healing mechanical efficiency and the results of this study are presented in [24].

Table 3. The ultrasound testing set-up based on embedded piezoelectric transducers.

Wave excitation set-up	Rectangular shape (P-wave)
Embedded transducer set-up	Amplitude = 800 Volts Duration = 2.5 μs Sampling rate = 10 MHz PZT patch (12 mm * 12 mm * 0.2 mm)

3.2 Acoustic emission

As discussed in previous studies, Acoustic Emission (AE) is able to locate the fracture phenomena in concrete and quantify the respective damage magnitude [25, 26]. Eight R15 sensors with a resonant frequency of 150 kHz are attached to concrete surface by means of magnetic holders. The AE sensors are placed at the central region of the concrete beam and their position is chosen in order to be able to monitor the damage restricted to the pre-notched section. The sensors capture all waves either emitted due to concrete damage process or the stress waves emitted by the embedded piezoelectric transmitter. Localization is naturally enabled for both groups of waves. Considering the waves emitted by the embedded transducers, the localization leads to the position of the transducers which are the actual sources. Since the position of the embedded transducers is constant, the possible differences in the localized sources through the AE algorithm, can directly lead to a quantification of the error as the test goes on and damage is accumulated.

The AEwin software is used to capture, locate and store the received stress waves. The AE set-up features are shown in Table 4. The AE sensor locations are graphically presented in Figure 2. The localization relies on the trilateration method that considers the arrival time of the propagated wave from several (at least four) sensors [25]. The wave speed and attenuation are measured at the healthy stage by means of pencil lead breakage and are presented in Table 4. The spatial 3D distance ($\Delta U_{isource}$) between the embedded transmitter (with coordinates X_u, Y_u, Z_u) and the AE sensors placed on concrete surfaces (with respecting coordinates X_i, Y_i, Z_i for i= 1 to 8 sensor's number) is calculated and shown in Figure 2a (red colored values). It is clear that AE localization takes place for all groups of waves.

Table 4. The Acoustic Emission testing set-up.

AE channels set-up	8 AE sensors (150 kHz resonance frequency)
AE Localization set-up	Threshold = 45 dB, pre-amplifier gain = 40 dB
	3D localization type
	Hits/Event : Min = 4 hits
	Wave velocity = 3800 m/s (pencil lead break test)
	Attenuation: y = 10dB/m (pencil lead break test)

3.3 Digital Image Correlation

The acoustic wave analysis is done in combination with the strain analysis obtained by Digital Image Correlation (DIC). DIC is commonly applied in concrete fracture studies since it provides full-field view of strain evolution at fractured areas and precise calculation of cracking size [27]. The method considers a pair of high-resolution cameras that provide a stereovision (3D) view and continuously capture images of the specimen surface during testing. The specimen surface is covered with a high-contrast black and white random speckle pattern that facilitates the images correlation. The Vic3D post-processing software provides full-field view of deformation and strain fields at different stages during testing (by comparing the reference and deformed concrete surface in the presence of cracks) [28]. The DIC technique is previously extensively used in our studies and further information can be found in [29, 4]. In this study, in combination with acoustic monitoring techniques, the integrated experimental set-up provides information regarding the crack evolution (crack nucleation, propagation, closure, reopening, etc.). The testing set-up features are summarized in Table 5. The basic information supplied by DIC in this study is the exact size of the crack opening at the bottom of the concrete beam. Additionally, DIC strain fields indicate the damage extent and location at different loading stages.

Table 5. The Digital Image Correlation testing set-up.

Cameras set-up	CCD Cameras, artificial illumination: halogen light
Image capturing set-up	Resolution = 2064 pixels x 2506 pixels
	Lenses focal length = 17 mm
	Area of interest = 100 mm x 100 mm
	Capturing rate = 0.5 Hz
	Subset = 21 pixels, Step = 6 pixels
	Strain filter window = 15 pixels

4. RESULTS

In Figure 3 the load-crack opening curves for both, reference (without encapsulated agent, grey color) and healing (black color) concrete beams are presented at the loading and reloading test stages. The DIC strain analysis in combination with fracture theory for concrete highlights the following crack propagation stages (marked with Roman numerals in Figure 3) [30, 31]:

I. Initially, the load-crack opening curve evolves linearly as the beam deforms elastically (stiffness).

II. The elastic deformation ends as micro-cracks form at the pre-crack and accumulate to a macro-crack.

III. The macro-crack forms across the beam's height as the flexural resistance is reached (ultimate load).

IV. The crack propagates and strain softening occurs (bilinear unloading-first part).

V. The crack cannot resist to opening and widens (bilinear unloading-second part).

The test was repeated after healing and the bars chart in Figure 3 presents the recovery of mechanical features at the reloading test by using the healing ratios n (%) described in equations 1 to 3:

$$n_{\text{fracture energy}}\,(\%) = \frac{Fracture\ toughness\ (reloading\ stage)}{Fracture\ toughness\ (loading\ stage)} * 100 \qquad \textbf{(eq.1)}$$

$$n_{\text{ultimate load}}\,(\%) = \frac{Ultimate\ load\ (reloading\ stage)}{Ultimate\ load\ (loading\ stage)} * 100 \qquad \textbf{(eq.2)}$$

$$n_{\text{stiffness}}\,(\%) = \frac{Initial\ stiffness\ (reloading\ stage)}{Initial\ stiffness\ (loading\ stage)} * 100 \qquad \textbf{(eq.3)}$$

The fracture energy in equation (1) is obtained according to the Rilem TC-50 FMC protocol [21] and the initial stiffness in equation (3) is calculated considering the early stage deformation of sample in response to the applied load.

It is shown that the concrete beams carrying healing agent recover their fracture energy, strength and stiffness up to 34, 37 and 89%, respectively. The filling of the crack void by means of released healing agent achieved both, sealing and partial mechanical restoration. This is not the case for the reference series, in which the mechanical recovery is poor as expected: the ultimate load at the reloading stage cannot overpass the load at the end of the loading stage and limited fracture energy and stiffness is measured. While other features like the mechanical response of the autonomously healed concrete beams and AE behavior are discussed in previous studies [6], [24] this study focuses on the source location calculation of the stress waves emitted by the embedded transmitter and how it is affected by the progressive damage of concrete.

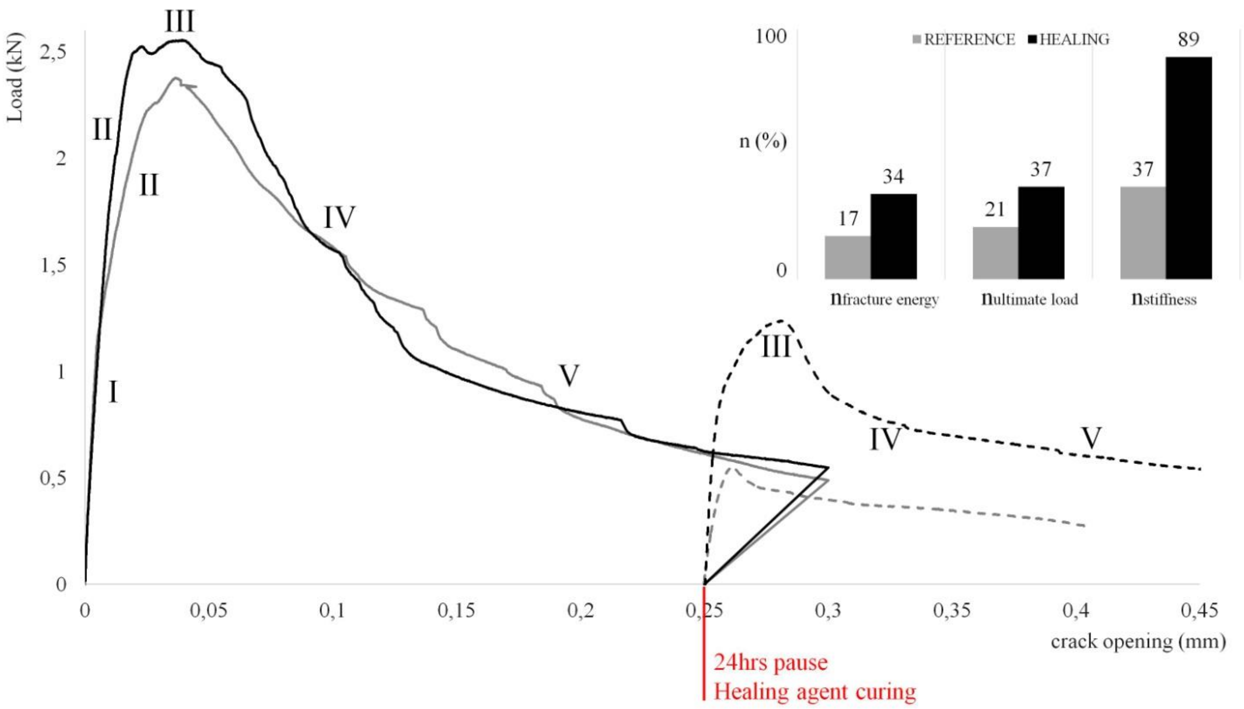

Figure 3. a) The load-crack opening graphs for both, reference (grey line) and healing (black line) specimens at loading and reloading test and the respective ratio of fracture energy, ultimate load and stiffness restoration after healing. The Roman numerals refer to the five stages that describe the progressive fracture process of concrete.

4.1 The clustering of AE activity based on the arrival time difference

In Figure 4, the time difference (Δt in μs) between the embedded transmitter emission and the AE hit received from each sensor is presented for the total amount of pulses captured during the loading test of the healing series (this loading test is chosen as a representative of the results). The points are marked with different colors indicating the respective AE sensor that receive the waves. The spatial 3D distance ($\Delta U_{isource}$) of each sensor from the source is provided as well.

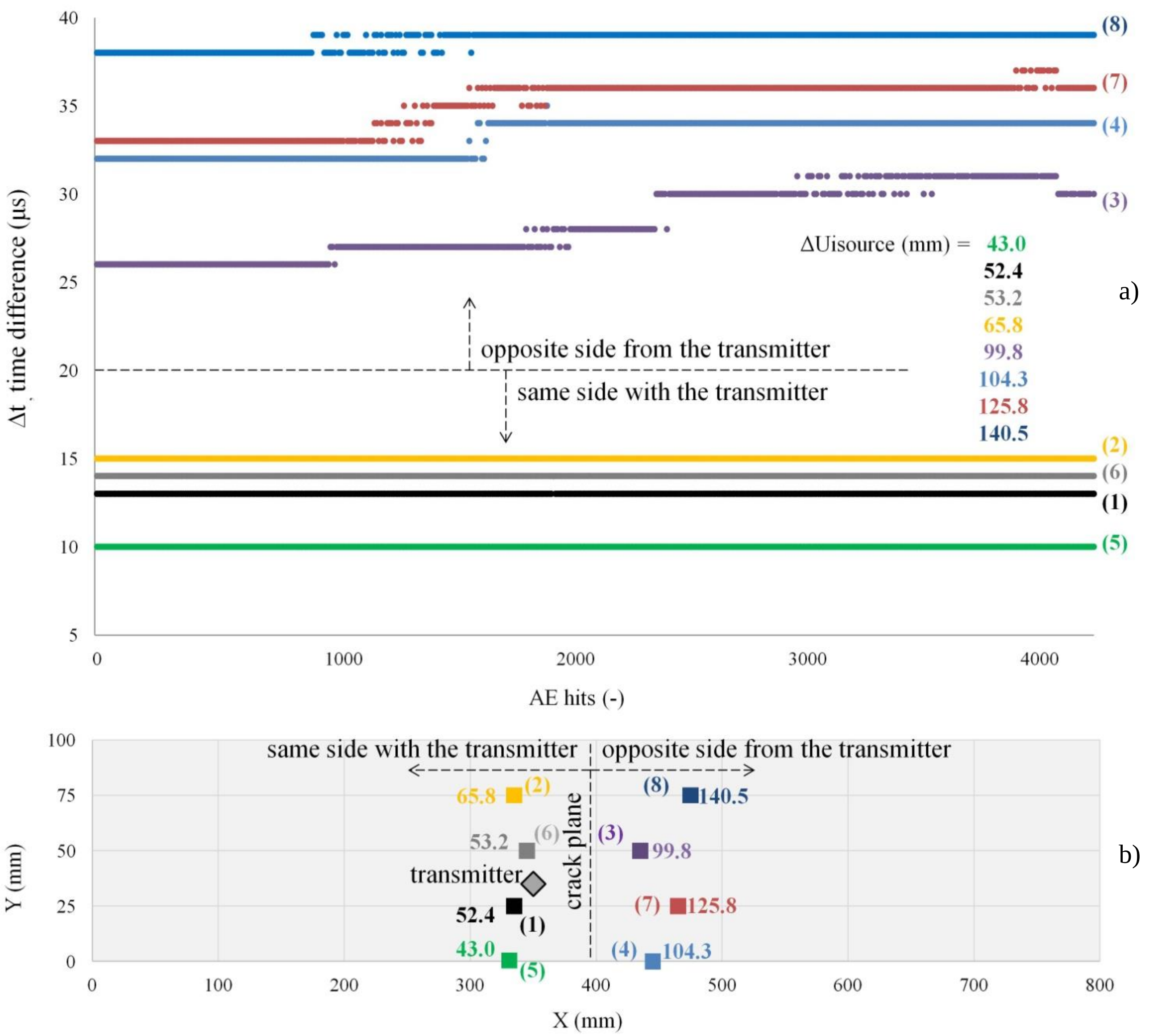

Figure 4. a) Time difference between the embedded transducer emission and the AE hits from each sensors (the respective spatial distance $\Delta U_{isource}$ is also given); b) For the sake of completeness, the sensors location is added.

The time difference remains constant for AE sensors placed at the side of the transmitter (#1, 2, 5 and 6) since no damage is developing between the embedded transducer and these sensors. Sensors which are at the opposite side (# 3, 4, 7 and 8) exhibit much greater time difference as the propagation distance is longer. In addition, it is obvious that the transit time to these sensors increases with time. This is due to the cracking that evolves and hinders wave propagation to the sensors on the other side of the crack. The increase of time delay does not appear instantly and at the same moment for all the AE sensors indicating that the different crack stages affect the arrival of the wave signals differently at sensors located at different heights. Nevertheless, for some of the sensors, the time delay increases up to 31.25% due to damage, which has considerable effect on the accuracy of localization. For this reason, the localization of AE wave source should be critically revised in the presence of cracks on concrete.

4.2 Evaluation of the source localization accuracy

In fracture theory and modeling, the crack is considered as a discontinuity following a three dimensional growth process [32]. In a similar approach, experimental studies using AE have shown that the accuracy of AE source localization is diminished as cracks occur [33]. With absolutely accurate localization the source should be detected constantly at the same point (position of the embedded transducer). The actual location of these AE events is projected on the X-Y plane and is presented in Figure 5 for the five stages of crack evolution (I-V, as defined in Figure 3). Only the middle zone of the beam, X coordinates limited to the range from 325 mm to 475 mm, where the crack occurs is shown in this figure. In parallel, the DIC strain ε_{xx} profiles are given for the corresponding crack stages. It is shown that the events localization gives (nearly) constant results up to stage III. Later, the accuracy decreases as the crack widens and reaches the top of the beam (stage IV, V) and the source is localized obviously away from the original fingerprint. In Figure 6 where the plots of difference between the actual coordinates of the source (X_{real}, Y_{real}, Z_{real}) and the ones obtained by AE during testing (X_{AE}, Y_{AE}, Z_{AE}) are given. The overall difference (Δ) that considers the three dimensional location difference is plotted as well.

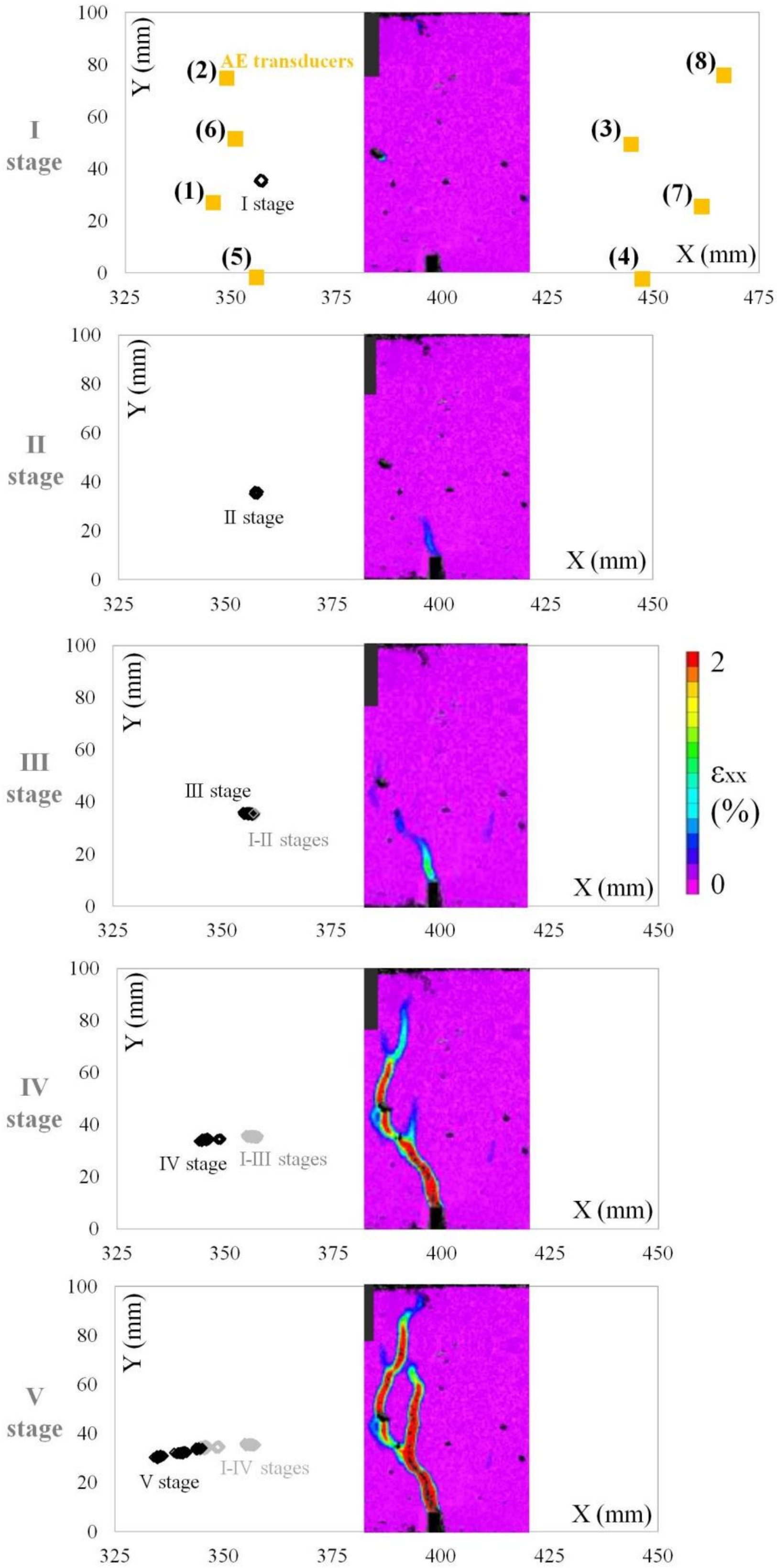

Figure 5. The AE events localization and the crack evolution based on DIC strain ε_{xx} profiles for the five stages of loading as projected on the X-Y plane (healing series).

It is observed that the loss of accuracy is greater for the X direction (black series, up to 18 mm). The loss of accuracy is lower for both, Y and Z direction (red and grey series respectively, up to 4 mm). It is shown that the three dimensional location difference (yellow series) is almost identical to the difference of the X coordinate. This phenomenon can be attributed to the fact that the crack is vertical to the X axis and influences most the wave propagation in this direction. Additionally, the X dimension of the specimen as well as the distance between the sensors and the AE source on the horizontal plane are longer, implying that a larger absolute error is reasonable. It is expected, the AE source localization would be more accurate if the AE sensors were placed covering a greater horizontal gauge length.

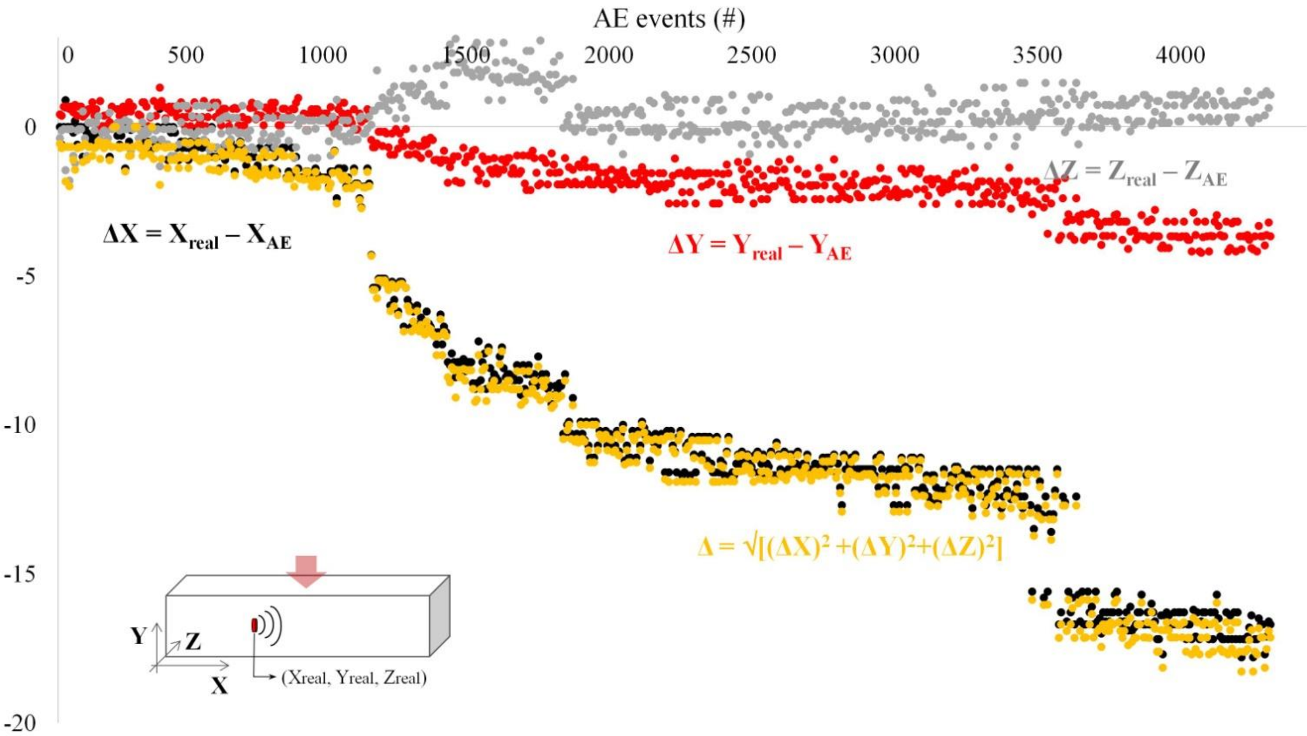

Figure 6. The AE events localization difference ΔX, ΔY, ΔX for X, Y, Z coordinates respectively during test.

At a step further, the three dimensional difference $\Delta D_{real-AE}$ (mm) between the source (X_{real}, Y_{real}, Z_{real}) and the one localized by AE sensors (X_{AE}, Y_{AE}, Y_{AE}) is plotted in Figure 7 versus the crack opening (measured by DIC) for both, the reference and healing series during loading and reloading tests. The difference $\Delta D_{real-AE}$ is divided by the distance between the two outermost sensors (#5 and #8), ΔD_{max} = 164 mm. This way, the difference is normalized considering a gauge length, the size of the area under investigation.

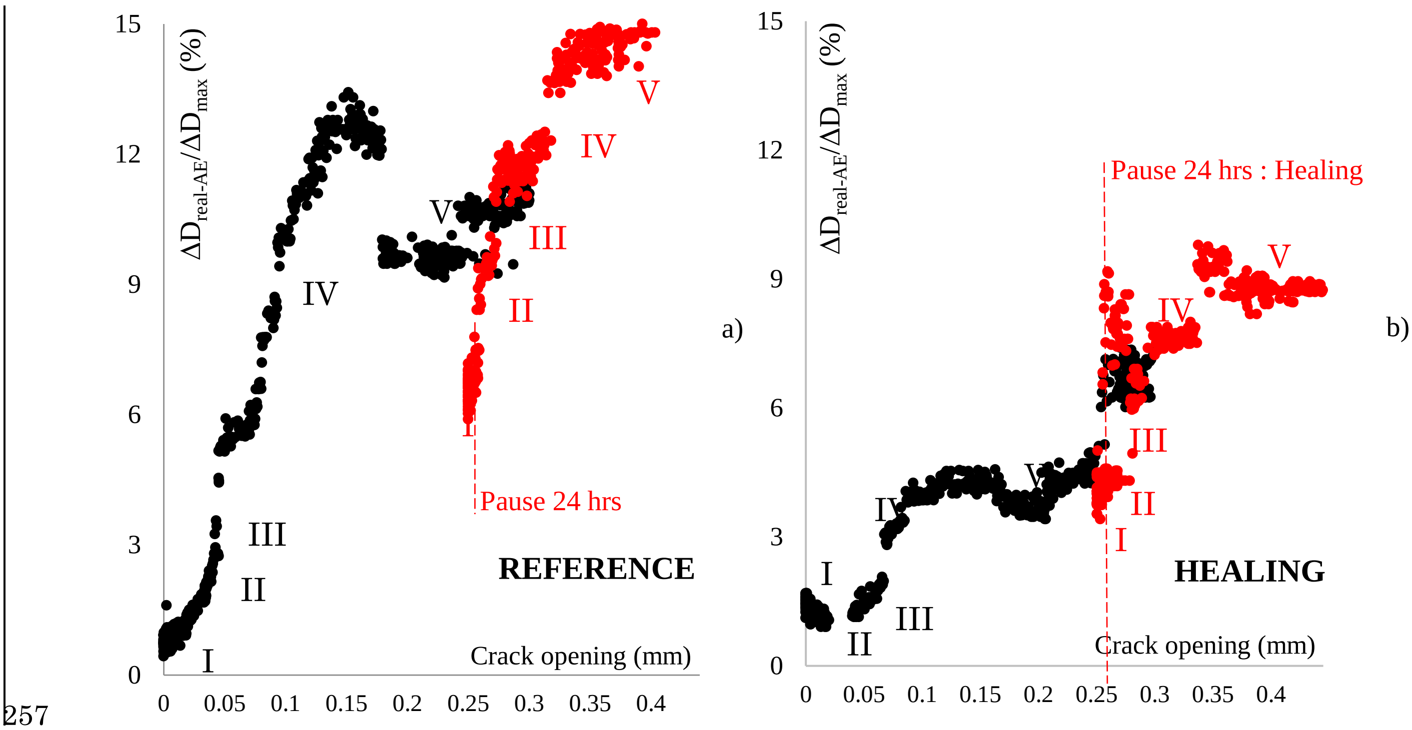

Figure 7. The normalized spatial difference $\Delta D_{real-AE}/\Delta D_{max}$ (%) between the source localization and the following ones during testing for the **a)** reference and **b)** healing series at loading (black spots) and reloading (red spots) tests versus the crack opening. The Roman numerals indicate the fracture stages as discussed in Figure 3.

The initial distance of the AE localization (in the sound specimens) relatively to the actual position of the source is around 1.25% (Figure 7 a, b). During the loading cycle in both cases, the cracking affects the velocity and transmission to all sensors and the $\Delta D_{real\text{-}AE}/\Delta D_{max}$ difference increases with damage. The error of accuracy is introduced when the peak load is reached and micro-cracks form (stage II). As macro-crack forms and propagates along the beam's height (stage III), the $\Delta D_{real\text{-}AE}/\Delta D_{max}$ error increases up to 3% and progressively increases up to 15% when the crack opening at the bottom of the beams is equal to 300 μm (strain-softening stages IV and V) and the crack reaches the top of the beam (see Table 6). In the healing case (Figure 7b), the capsules breakage affects the accuracy pulse localization. It is shown that after the load peak (stage IV) the capsules resist to damage propagation (crack's length is limited to 12 mm – see Table 6) and build up a local reinforcement that contributes to material's toughness and lead to almost constant values of the $\Delta D_{real\text{-}AE}/\Delta D_{max}$ difference.

At the beginning of the reloading cycle, the error is reduced for both series since the load is eliminated and the crack opening is diminished from 300 μm to approximately 250 μm (Figure 7a, b). In the reference case, the $\Delta D_{real\text{-}AE}/\Delta D_{max}$ increases up to 10% as the ultimate load is reached (Figure 7a) and the crack propagates up to the top of the beam (Table 6). The latter indicates no resistance of the reference beam to fracture.

In the healing case (Figure 7b), the error is significantly diminished after the autonomous repair: from 9% at the end of the loading cycle to 3.4% at the beginning of the reloading cycle something that may also be attributed to the action of the healing agent. Due to great stiffness restoration after healing, the $\Delta D_{real\text{-}AE}/\Delta D_{max}$ difference remains almost stable (up to 4.9%) till the crack reopening. It is proven that the polymerized polyurethane seals the crack and provides a solid path for the wave propagation and therefore restores to some better extend the accuracy of localization. However, as soon as the ultimate strength of the healed beam is reached, the crack reopens, propagates till the top of the sample and the $\Delta D_{real\text{-}AE}/\Delta D_{max}$ difference notably increases indicating no further resistance of the beam to damage.

For the sake of completeness, the overview of the $\Delta D_{real\text{-}AE}/\Delta D_{max}$ (%) difference values and the length of the crack measured for the reference sample and the three healing samples (PU1, PU2, and PU3) at different stages of damage are given in Table 6.

Table 6. $\Delta D_{real\text{-}AE}/\Delta D_{max}$ difference and the crack length overview.

		REF		**PU1**		**PU2**		**PU3**	
		$\Delta D_{real\text{-}AE}/\Delta D_{max}$ (%)	Crack length (mm)	$\Delta D_{real\text{-}AE}/\Delta D_{max}$ (%)	Crack length (mm)	$\Delta D_{real\text{-}AE}/\Delta D_{max}$ (%)	Crack length (mm)	$\Delta D_{real\text{-}AE}/\Delta D_{max}$ (%)	Crack length (mm)
LOAD	Start of stage I	1.0	0	1.25	0	0.5	0	1.25	0
	End of stage II	3.0	32	1.3	12	0.95	10	1.2	12
	End of stage IV	8.9	65	3.8	60	4.7	59	5.4	55
	End of stage V	15	80	9.0	75	8.0	70	10.7	68
RELOAD	Start of stage I	6.8	0	3.4	0	1.0	0	4.2	0
	End of stage II	7.6	30	4.9	0	0.9	0	6.0	0
	End of stage IV	10.0	80	7.75	66	4.0	70	9.0	59
	End of stage V	15.0	80	10.3	75	4.2	70	11.0	68

5. DISCUSSION and CONCLUSIONS

The analyses of the crack patterns on concrete have shown that under service load, several cracks dynamically interact [34]. In previous studies evaluating the healing performance of concrete, it is shown that a crack can open wider at the same moment that another crack at the close vicinity heals and closes [35, 36, 37]. These dynamic simultaneous crack phenomena introduce complexity that weakens the two main assumptions of AE localization theory:

- The location of the AE source is obtained considering homogeneous medium properties, therefore stable wave velocity [38]**.** The wave velocity decreases in the presence of open cracks. As these cracks are filled with polymerized healing agent, a thin intersection of material with different wave velocity should be considered.
- There is only a direct path between the wave source and the AE sensor. Dynamic crack nucleation, and propagation introduce discontinuities at different scales: from the micro-cracks formed at the fracture process zone surrounding the crack till the macro-crack that propagates in space. The scattering effect cannot be eliminated.

Suitable localization accuracy is important for the automated (autonomous healing) repetitive detection and repair of cracks on concrete [39, 8]. The 3D healing network forms a dense mesh of tubes that remain empty during the service life of the concrete element. The agent is kept on a reservoir system and is delivered at the damaged zone only as soon as one of the tubes fails due to cracking. The crack nucleation and propagation will lead to tube's rupture and the healing agent delivery will be accomplished as soon as the automated healing system detects accurately the position of damage. Only in this case, the correct tube will be activated and filled with healing agent that seals the crack void. For a realistic AE gauge length dimension of 2 m, the localization error measured up to about 10% allows for an accuracy of 200 mm in absolute length even at a severely damaged state. This is considered adequate as the distance between successive vanes of a network system could not be less than 150 mm, in order not to compromise the load bearing capacity of the structure. In this case the validation of the accuracy was done by the use of an embedded pulser, the position of which was known a priori. This was a suitable calibrating method that enabled to accurately measure the resulted error.

As a conclusion, the study concerns the evaluation of the AE localization accuracy for the case of a crack that forms on lab-scale concrete beams, propagates and is sealed in the presence of autonomous healing mechanism. As expected, standard AE source localization technique accurately provides the source location in sound sample, but the localization accuracy declines as damage develops. The error of the source localization is quantified in respect to the crack evolution stages (micro-cracking up to macro-crack) and the gauge length. It is shown that the error remains up to the order of 10% of the gauge length even at severely damaged stage. This accuracy is adequate as it is deemed essential for activation of the healing at the correct zone in the case of non-visible cracks in the volume of the component.

Acknowledgements. The authors are grateful to SIM (Strategic Initiative Materials Flanders) program on Engineered Self-Healing Materials (SHE) for providing financial support.

REFERENCES

[1] D. McCann and M. Forde, "Review of NDT methods in the assessment of concrete and masonry structures," *NDT & E International,* pp. 71-84, 2001.

[2] B. Tremper, "Repair of damaged concrete with epoxy resins," *ACI Journal Proceedings,* vol. 57, no. 8,

pp. 173-182, 1960.

[3] K. Van Tittelboom and N. De Belie, "Self-Healing in Cementitious Materials—A Review," *Materials,* vol. 6, pp. 2182-2217, 2013.

[4] E. Tsangouri, D. Aggelis, K. Van Tittelboom, N. De Belie and D. Van Hemelrijck, "Detecting the Activation of a Self-Healing Mechanism in Concrete by Acoustic Emission and Digital Image Correlation," *The Scientific World Journal,* no. 424560, 2013.

[5] G. Karaiskos, A. Deraemaeker, D. Aggelis and D. Van Hemelrijck, "Monitoring of concrete structures using the ultrasonic pulse velocity method," *Smart Materials and Structures,* vol. 24, no. 11, p. 113001, 2015.

[6] E. Tsangouri, Experimental assessment of fracture and autonomous healing of polymer and concrete systems, Brussels: Free University Press., 2015.

[7] K. Van Tittelboom, E. Tsangouri, D. Van Hemelrijck and N. De Belie, "The efficiency of self-healing concrete using more realistic manufacturing procedures and crack patterns," *Cement and concrete composites,* vol. 57, pp. 142-152, 2014.

[8] G. Thierens and G. De Valck, "Feasibility of up-scaling and implementing self-healing concrete in real-life applications," Free University of Brussels (VUB), Brussels, Belgium, 2014.

[9] K. Van Breugel, "Is there a market for self-healing cement-based materials," in *First International Conference on Self Healing Materials (ICSHM)*, Delft, The Netherlands, 2007.

[10] G. Karaiskos, E. Tsangouri, D. Aggelis, K. Van Tittelboom, N. De Belie and D. Van Hemelrijck, "Performance monitoring of large-scale autonomously healed concrete beams under four-point bending through multiple non-destructive testing methods," *Smart Materials and Structures,* vol. 25, p. 055003, 2016.

[11] K. Komlos, S. Popovics, T. Nurnbergerova, B. Babal and J. Popovics, "Ultrasonic pulse velocity test of concrete properties as specified in various standards," *Cement and Concrete Composites,* vol. 18, no. 5, pp. 357-364, 1996.

[12] C. Grosse and M. Ohtsu, Acoustic emission testing, Springer Science & Business Media, 2008, p. 402.

[13] D. Aggelis and T. Shiotani, "Repair evaluation of concrete cracks using surface and through-transmission wave measurements," *Cement and Concrete Composites,* vol. 29, pp. 700-711, 2007.

[14] H. Reinhardt, C. Grosse and T. Dahm, "Localization and classification of fracture types in concrete with quantitative acoustic emission measurement techniques," *NDT and E International,* vol. 30, no. 4, pp. 223-230, 1997.

[15] K. Chai, D. Aggelis, S. Momoki, T. Shiotani and Y. Kobayashi, "Large-scale evaluation of concrete repair by three-dimensional elastic- wave-based visualization technique," *Structural Health Monitoring,* vol. 12, pp. 240-251, 2013.

[16] M. Shigeishia, S. Colombo, K. Broughtonb, H. Rutledgeb, A. Batchelorb and M. Forde, "Acoustic emission to assess and monitor the integrity of bridges," *Construction and Building Materials,* vol. 15,

no. 1, pp. 35-49, 2001.

[17] S. Rouchier, G. Foray, N. Godin, M. Woloszyn and J.-J. Roux, "Damage monitoring in fibre reinforced mortar by combined digital image correlation and acoustic emission," *Construction and Building Materials,* vol. 38, pp. 371-380, 2013.

[18] Q. Han, J. Xu, A. Carpinteri and G. Lacidogna, "Localization of acoustic emission sources in structural health monitoring of masonry bridge," *Structural Control and Health Monitoring,* vol. 22, no. 2, pp. 314-329, 2015.

[19] A. Carpinteri, J. Xu, G. Lacidogna and A. Manuello, "Reliable onset time determination and source location of acoustic emissions in concrete structures," *Cement and Concrete Composites,* vol. 34, no. 4, pp. 529-537, 2012.

[20] Z. Bazant and H. Byung, "Crack band theory for fracture of concrete," *Materiaux et constructions,* vol. 16, no. 3, pp. 155-177, 1983.

[21] T. Rilem 50-FMC, "Determination of the Fracture Energy of Mortar and Concrete by Means of Three-point Bend Tests on Notched Beams," *Materials and Structures,* vol. 18, pp. 285-290, 1985.

[22] G. Song, H. Gu, Y. Mo, T. Hsu and H. Dhonde, "Concrete structural health monitoring using embedded piezoceramic transducers," *Smart Materials and Structures,* vol. 16, no. 4, p. 959, 2007.

[23] C. Dumoulin, G. Karaiskos, J.-Y. Sener and A. Deraemaeker, "Online monitoring of cracking in concrete structures using embedded piezoelectric transducers," *Smart Materials and Structures,* vol. 23, no. 115016, 2014.

[24] E. Tsangouri, G. Karaiskos, D. Aggelis and A. Deraemaeker, "Crack sealing and damage recovery monitoring of a concrete healing system using embedded piezoelectric transducers," *Structural Health Monitoring,* no. 1475921715596219, 2015.

[25] R. Miller and P. Mc Intire, Acoustic Emission Testing NDT Handbook, vol. 5, American Society for Non-destructive Testing, 1987, p. 652.

[26] A. Carpinteri, G. Lacidogna, M. Corrado and E. Di Battista, "Cracking and crackling in concrete-like materials: A dynamic energy balance," *Engineering Fracture Mechanics,* vol. 155, pp. 130-144, 2016.

[27] S. Shah and S. Choi, "Non-destructive techniques for studying fracture processes in concrete," *International Journal of Fracture,* vol. 98, pp. 3-4, 1999.

[28] J. Orteu, M. Sutton and H. Schreier, Image Correlation for Shape, Motion and Deformation Measurements: Basic Concepts, Theory and Applications, Springer, 2009, p. 322.

[29] D. Aggelis, S. Verbruggen, E. Tsangouri, T. Tysmans and D. Van Hemelrijck, "Characterization of mechanical performance of concrete beams with external reinforcement by acoustic emission and digital image correlation," *Construction and Building Materials,* vol. 47, pp. 1037-1045, 2013.

[30] J. Van Mier, Fracture process of concrete: Assessment of material parameters for fracture models, CRC Press, 1997, p. 446.

[31] E. Gdoutos, Fracture Mechanics An Introduction Series: Solid Mechanics and Its Applications, 2005.

[32] A. Griffith, "The phenomena of rupture and flow in solids," *Philosophical Transactions of the Royal Society A: Mathematical, Physical and Engineering Sciences,* vol. 221, pp. 163-198, 1921.

[33] A. Maji and S. Shah, "Process zone and acoustic-emission measurements in concrete," *Experimental mechanics,* vol. 28, no. 1, pp. 27-33, 1988.

[34] S. Zihai, Crack Analysis in Structural Concrete, Theory and Applications, Elsevier, 2009, p. 344.

[35] K. Van Tittelboom, N. De Belie, F. Lehmann and C. Grosse, "Acoustic emission analysis for the quantification of autonomous crack healing in concrete," *Construction and Building Materials,* vol. 28, no. 1, p. 333–341, 2012.

[36] S. Granger, A. Loukili, G. Pijaudier-Cabot and G. Chanvillard, "Experimental characterization of the self-healing of cracks in an ultra-high performance cementitious material: Mechanical tests and acoustic emission analysis," *Cement and Concrete Research,* vol. 37, no. 4, pp. 519-527, 2007.

[37] K. Van Tittelboom, J. Wang, A. Gomes Araujo, D. Snoeck, E. Gruyaerta, B. Debbaut, H. Derluyn, E. Tsangouri, D. Van Hemelrijck and N. De Belie, "Comparison of different approaches for self-healing concrete in a large-scale lab test," *Construction and Building Materials,* vol. 107, pp. 125-137, 2016.

[38] T. Schumacher, D. Straub and C. Higgins, "Toward a probabilistic acoustic emission source," *Journal of Sound and Vibration,* vol. 19, no. 10, pp. 4233-4245, 2012.

[39] N. Bensilam and Y. Zouhair, "Strength variation in relation to self-healing efficiency in self-healing concrete," Free University of Brussels (VUB), Brussels, Belgium, 2015.